Improved Measurement of the Hydrogen 1S–2S Transition Frequency

Christian G. Parthey,[1] Arthur Matveev,[1] Janis Alnis,[1] Birgitta Bernhardt,[1] Axel Beyer,[1] Ronald Holzwarth,[1,*] Aliaksei Maistrou,[1] Randolf Pohl,[1] Katharina Predehl,[1] Thomas Udem,[1] Tobias Wilken,[1] Nikolai Kolachevsky,[1,†] Michel Abgrall,[2] Daniele Rovera,[2] Christophe Salomon,[3] Philippe Laurent,[2] and Theodor W. Hänsch[1,‡]

[1]*Max-Planck-Institut für Quantenoptik, 85748 Garching, Germany*
[2]*LNE-SYRTE, Observatoire de Paris, 61 avenue de l'Observatoire, 75014 Paris, France*
[3]*Laboratoire Kastler-Brossel, CNRS, 24 rue Lhomond, 75231 Paris, France*

(Received 15 July 2011; published 11 November 2011)

We have measured the 1S–2S transition frequency in atomic hydrogen via two-photon spectroscopy on a 5.8 K atomic beam. We obtain $f_{1S-2S} = 2\,466\,061\,413\,187\,035\,(10)$ Hz for the hyperfine centroid, in agreement with, but 3.3 times better than the previous result [M. Fischer *et al.*, Phys. Rev. Lett. **92**, 230802 (2004)]. The improvement to a fractional frequency uncertainty of 4.2×10^{-15} arises mainly from an improved stability of the spectroscopy laser, and a better determination of the main systematic uncertainties, namely, the second order Doppler and ac and dc Stark shifts. The probe laser frequency was phase coherently linked to the mobile cesium fountain clock FOM via a frequency comb.

DOI: 10.1103/PhysRevLett.107.203001 PACS numbers: 32.30.Jc, 06.20.Jr, 42.62.Fi

For the last six decades, spectroscopy on atomic hydrogen with its calculable atomic structure has been fueling the development and testing of quantum electrodynamics (QED) and has led to a precise determination of the Rydberg constant and the proton charge radius [1]. The absolute frequency of the 1S–2S transition has been measured with particularly high precision and has become a corner stone in the least squares adjustment of the fundamental constants [2]. The resonance has been used to set limits on a possible variation of fundamental constants [3] and violation of Lorentz boost invariance [4]. It further promises a stringent test of the charge conjugation, parity, and time (CPT) reversal theorem by comparison with the same transition in antihydrogen [5,6].

In this Letter we present a more than 3 times more accurate measurement of the 1S–2S transition as compared to the previous best measurements [3,7], now reaching a relative uncertainty of 4.2×10^{-15}. The key improvements are (a) the replacement of a dye laser with a diode laser system with improved frequency stability for the two-photon spectroscopy, (b) a direct measurement of the 2S velocity distribution of the thermal atomic hydrogen beam which allows a more accurate characterization of the second order Doppler effect (SOD), and (c) the introduction of a quench laser, resetting the population to the ground state 1 cm after the hydrogen nozzle, removing possible frequency shifts due to the high density of atoms and a possible dc Stark shift from patch charges within the nozzle.

The extended-cavity diode spectroscopy laser system (ECDL) has been described elsewhere [8]. An ECDL master oscillator near 972 nm is amplified in a tapered amplifier. The laser radiation is frequency doubled twice within two resonant cavities to obtain 13 mW of the required uv light near 243 nm. Locking the laser to a high finesse cavity made from ultralow expansion glass leads to a linewidth of less than 1 Hz and a fractional frequency drift of 1.6×10^{-16} s^{-1} [9]. A fiber laser frequency comb with a repetition rate of 250 MHz is used to phase-coherently link the cavity frequency to an active hydrogen maser which is calibrated using the mobile cesium fountain atomic clock FOM [10]. We apply cycle slip detection as described in [11].

The beam apparatus (Fig. 1) follows the design of [12] and has been used before [13]. Hydrogen is dissociated at a pressure of 1 mbar in a radio frequency (rf) discharge running in a sapphire tube. A Teflon capillary controls the flow and Teflon tubing guides the atomic hydrogen to a copper nozzle cooled to 5.8 K by a liquid helium flow cryostat. The dissociation fraction at the nozzle (2.2 mm diameter) is about 10%. After 45 min of operation, the

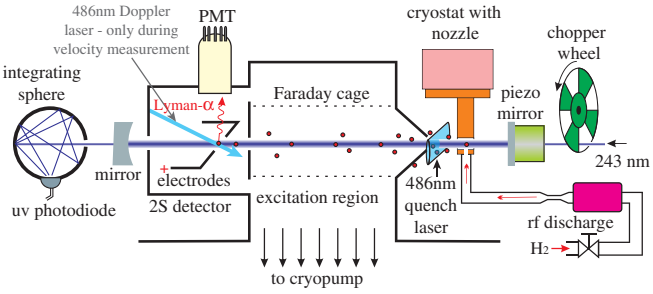

FIG. 1 (color online). Schematic of the beam apparatus. A standing laser wave at 243 nm (between gray mirrors) with a $1/e^2$ waist radius of $w_0 = 292$ μm at the flat cavity front mirror excites the sharp 1S–2S transition in a collinearly propagating cold thermal beam of atomic hydrogen emerging from a cooled copper nozzle. The 2S state is detected after quenching with a localized electric field which releases a Lyman-α photon. See text for further details.

nozzle closes up with frozen molecular hydrogen. We then heat it to 20 K for 15 min to evaporate the hydrogen molecules. The atomic beam is defined by a 2.4 mm (front) and a 2.1 mm (rear) diameter aperture which also separate the differentially pumped excitation region (10^{-5} mbar/10^{-8} mbar). This region is shielded by a grounded Faraday cage from electric stray fields that may build up from laser ionized hydrogen and due to uv stray light. An enhancement cavity forms a standing wave for collinear excitation of the $1S$–$2S$ transition by two counter-propagating photons. For detection, excited, metastable atoms are quenched via the $2P$ state by an electric field (10 V/cm) and the emitted 121 nm photons are detected by a photomultiplier tube (PMT). The intracavity power is monitored by measuring the transmission of the cavity using a photodiode connected to an integrating sphere.

During 12 consecutive days starting on May 30, 2010, with a break on June 9, 1587 $1S$–$2S$ spectra have been recorded (see Fig. 2). For each $1S$–$2S$ line the spectroscopy laser's frequency samples the transition in random order. At each frequency point we count Lyman-α photons for 1 s (with a 50% duty cycle due to the chopper, see below) at two different 243 nm laser intensities. A double-pass acousto-optic modulator (AOM) in zeroth order placed in front of the enhancement cavity allows us to quickly alter the power level under otherwise identical conditions to correct for the ac Stark effect (see below). After switching the AOM we wait several milliseconds to avoid possible frequency chirps.

We apply an external magnetic field of 0.5 mT to separate the magnetic components. For the spectroscopy, we use the transitions from $F = 1$, $m_F = \pm 1$ to $F' = 1$, $m_{F'} = \pm 1$ whose Zeeman shifts of the ground and excited state almost completely cancel. The hyperfine

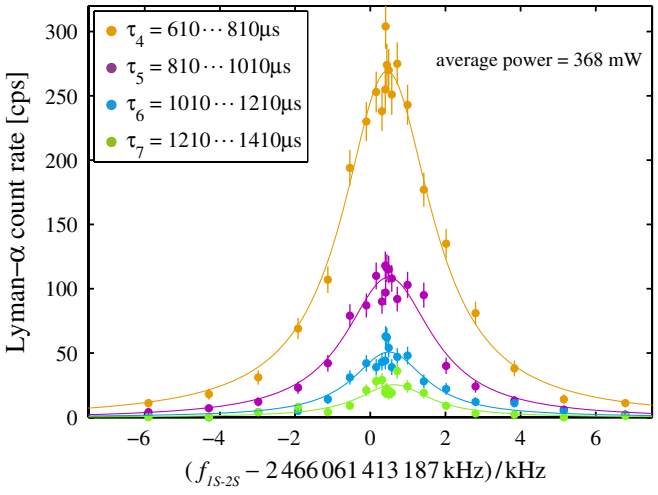

FIG. 2 (color online). Single scan line profile for different delays along with Lorentzian fits. With the detection delay τ, we set an upper limit on the atoms velocity but reduce the signal accordingly. The full width at half maximum (FWHM) is about 2 kHz.

centroid frequency is obtained by adding $\Delta f_{\mathrm{HFS}} = +310\,712\,229.4\,(1.7)$ Hz calculated from the experimental results for the $1S$ and $2S$ hyperfine splittings [14,15].

Next, we discuss the compensation of the two main systematic effects and estimations of the remainder. The Doppler effect, due to the velocity v of the atoms, is canceled to first order by virtue of the two-photon excitation scheme [16]. The remaining second order Doppler shift $\Delta f_{\mathrm{dp}} = -v^2 f_{1S-2S}/(2c^2)$ is compensated in two steps: First, we chop the excitation light at 160 Hz (see Fig. 1) which allows time-of-flight resolved detection of atoms excited to the $2S$ state. Evaluating only $2S$ counts recorded at a certain delay τ after the light has been switched off by the chopper wheel, allows the fastest atoms to escape. This samples the slow tail of the velocity distribution and removes most of the SOD. Second, to further study and subtract the SOD, we have independently measured the velocity distribution of the $2S$ atoms as described below. We evaluate the resonance data in each of the 12 time-of-flight ranges $\tau_1 = 10\cdots210$ μs, $\tau_2 = 210\cdots410$ μs, …, $\tau_{12} = 2210\cdots2410$ μs independently, which provides a test of the SOD correction. The residual uncertainty of this procedure was determined by evaluating a second data set that was generated using a Monte Carlo (MC) simulation [17,18] in exactly the same way. For various simulation parameters such as temperature, geometry, and initial $1S$ velocity distributions we find the uncertainty to be smaller than 2.0×10^{-15} which is below the current statistical uncertainty of 2.6×10^{-15} (see Table I).

TABLE I. Uncertainty budget for hydrogen frequency $f_{1S-2S} \approx 2.466 \times 10^{15}$ Hz. The observed linewidth is 2 kHz FWHM.

	σ [Hz]	σ/f_{1S-2S} [10^{-15}]
Statistics	6.3	2.6
2nd order Doppler effect	5.1	2.0
Line shape model	5.0	2.0
Quadratic ac Stark shift (243 nm)	2.0	0.8
ac Stark shift, 486 nm quench light	2.0	0.8
Hyperfine correction	1.7	0.69
dc Stark effect	1.0	0.4
ac Stark shift, 486 nm scattered light	1.0	0.4
Zeeman shift	0.93	0.38
Pressure shift	0.5	0.2
Blackbody radiation shift	0.3	0.12
Power modulation AOM chirp	0.3	0.11
rf discharge ac Stark shift	0.03	0.012
Higher order modes	0.03	0.012
Line pulling by $m_F = 0$ component	0.004	0.0016
Recoil shift	0.009	0.0036
FOM	2.0	0.81
Gravitational redshift	0.04	0.077
Total	10.4	4.2

The second systematic effect that needs to be corrected for is the ac Stark shift which is mostly linear in laser power P. However, a small quadratic contribution [17] must be taken into account before we can apply a linear extrapolation using the stable, but otherwise not precisely calibrated laser power readings. The main contribution to this nonlinear ac Stark shift is due to ionization of the $2S$ atoms by a third 243 nm photon that removes preferably atoms that see larger laser powers. For excitation laser powers of 300 mW as present in our experiment the quadratic ac Stark shift contributes on the order of 1×10^{-14} as derived from the MC simulations. This is sufficiently small to rely on these simulations that assume a Maxwell distribution for the $1S$ atoms using the absolute laser power within 20% relative uncertainty. Modeling and subtracting the delay-dependent quadratic ac Stark effect in this way then allows us to linearly extrapolate the line centers. This procedure removes the ac Stark shift with an uncertainty of 0.8×10^{-15}.

We find the experimental (and simulated) line centers by fitting Lorentzians which represent a good approximation of the line shape for delays $\tau_4 = 610 \cdots 810$ μs and higher (see Fig. 2). For lower delays the SOD causes an asymmetry so we do not evaluate them. A small residual asymmetry for the longer delays is determined and taken into account by comparing with the MC simulation. Again, we use this simulation only for small corrections.

To correct the SOD $\Delta f_{\mathrm{dp}} = -v^2 f_{1S-2S}/(2c^2)$, an accurate understanding of the velocity distribution is desirable. Previously, this information has been extracted from the line shape of the $2S$ spectra with an uncertainty of 8×10^{-15} [7]. Here, we measure the $2S$ velocity distribution directly via the first order Doppler effect on the $2S$–$4P$ one-photon transition near 486 nm which we excite at an angle of 45° with respect to the hydrogen beam (Doppler laser in Fig. 1). The $2S$–$4P$ transition has a sufficiently narrow natural linewidth of 13 MHz (corresponding to $\Delta v =$ 8 m/s at 45°) to resolve velocities on the level of 1 m/s.

The $4P$ state decays to the ground state with a 90% branching ratio emitting a 97 nm Lyman-γ photon which can be easily detected using a channeltron. Pulsing the 486 nm Doppler laser with an AOM avoids power broadening (and loss of velocity resolution) while providing equal quench probability for atoms of different velocity. We cross the 486 nm beam with the atomic beam right between the quench electrodes which are grounded for the velocity distribution measurements. Using the same delayed detection as for the $1S$–$2S$ spectra allows to extract the velocity distribution of $2S$ atoms that contribute to the signal with delay τ. Observing the excited state directly gives the advantage of measuring the convolution of the velocity distribution with the excitation probability making the simulation of $1S$–$2S$ excitation dynamics unnecessary for this purpose. The low velocity part of a typical Doppler profile for delays $\tau_4 = 610 \cdots 810$ μs to $\tau_7 = 1210 \cdots 1410$ μs is shown in Fig. 3(a).

From 131 recorded Doppler profiles $p_\tau(v, P)$ we calculate the SOD for each delay τ according to $\Delta f_{\mathrm{dp}}(P) = -v_c^2(P) f_{1S-2S}/(2c^2)$ where the central velocity v_c is determined by a Gaussian fit to the velocity profiles [see Fig. 3(a)]. The power dependence arises from ionization losses of slow atoms. A linear fit to $\Delta f_{\mathrm{dp}}(P)$ reveals the SOD correction as shown in Fig. 3(b).

The uncertainty in the second order Doppler correction is caused by three main sources. First, the statistical uncertainty obtained from linear regression analysis of $\Delta f_{\mathrm{dp}}(P)$ contributes 1.7×10^{-15}. Second, during the velocity measurements the $1S$–$2S$ spectroscopy laser was kept on the resonance only within ± 160 Hz. MC simulation reveals an associated uncertainty of 0.8×10^{-15}. Third, the 45° angle between the atomic beam and the laser beam used to measure the velocity distribution can only be adjusted within $\pm 1°$. This translates to an uncertainty in the SOD of 0.8×10^{-15}. Summing in quadrature leads to an overall uncertainty of the second order Doppler correction of 2.0×10^{-15}.

The fully corrected data are shown in Fig. 4. The transition frequency f_{1S-2S} is independent of the delay for $\tau_4 = 610 \cdots 810$ μs to $\tau_7 = 1210 \cdots 1410$ μs unlike before the correction. For the final analysis we only use delays τ_5 and τ_6. For delays $\tau_{1 \cdots 4}$ the SOD cannot be

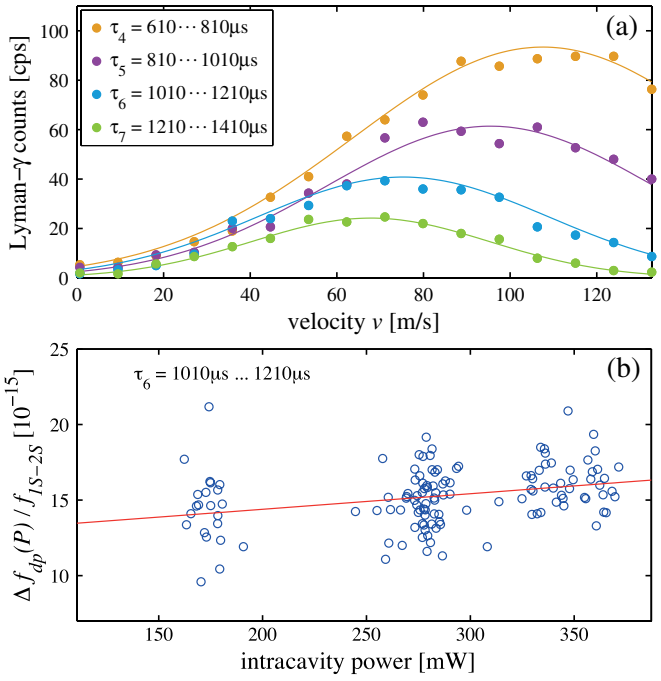

FIG. 3 (color online). (a) Low velocity part of the Doppler profiles of $2S$ atoms recorded for different delays τ at 370 mW intracavity power along with Gaussian fit. (b) Fractional second order Doppler correction $\Delta f_{\mathrm{dp}}(P)/f_{1S-2S}$ versus intracavity power for delay $\tau_6 = 1010$ μs $\cdots$ 1210 μs. Each point represents the Doppler correction as calculated from the central velocity of a single velocity profile measurement along with a linear fit.

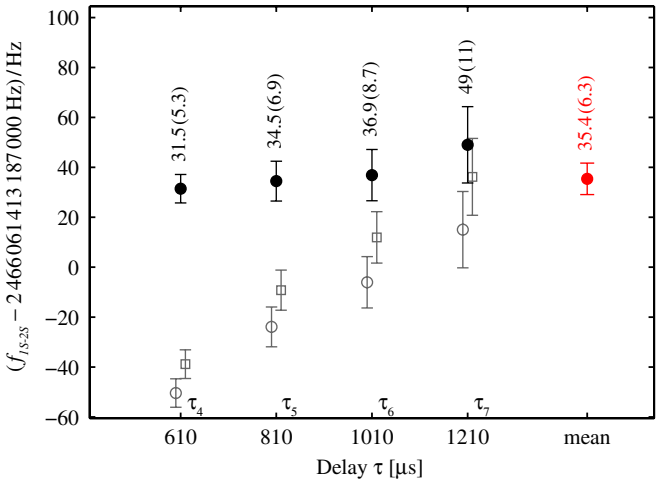

FIG. 4 (color online). The plot shows $f_{1S\text{–}2S}$ with all corrections applied for delays $\tau_4 = 610 \cdots 810$ μs to $\tau_7 = 1210 \cdots 1410$ μs (filled points) along with the mean as calculated from delays $\tau_{5,6}$ (see text). The error bars represent the 1σ statistical uncertainty. The open circles show the same data with the second order Doppler effect not corrected, the open squares include neither the second order Doppler effect nor the quadratic ac Stark shift corrections.

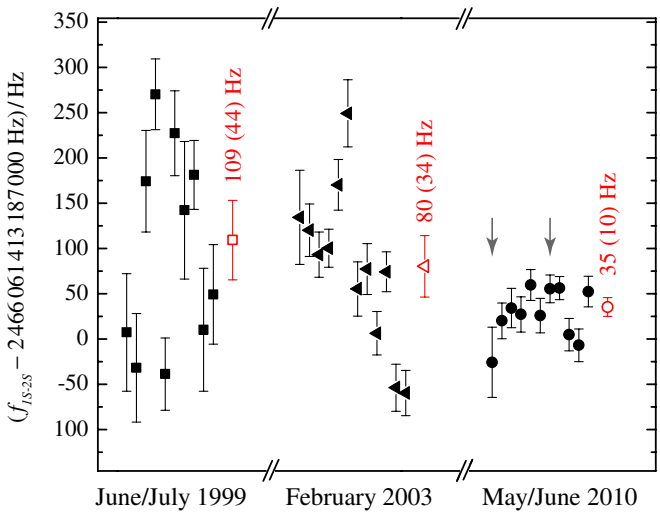

FIG. 5 (color online). The $1S$–$2S$ centroid frequency of the current measurement is compared with the previous two measurements [3,7]. The filled points represent an average per day, the open points (with label) are the final values. Their error bars represent the total 1σ uncertainty. The arrows indicate the measurements directly after refreshing the graphite coating of the excitation region and of the Faraday cage.

sufficiently characterized. For delay τ_7 and higher, the quadratic ac Stark shift correction cannot be extracted with competitive uncertainty due to the inaccuracy of the absolute power measurement.

As mentioned above, the pressure shift and the dc Stark effect have been greatly reduced as compared to [13] by the introduction of the quench laser. With an atom flux of 10^{17} particles per second we find the remaining pressure shift within the excitation region to be well below 0.2×10^{-15} [19]. In [20] the remaining dc Stark shift was measured to be 0.4×10^{-15}.

Scattered light from the 486 nm quench beam can cause an ac Stark shift on the $1S$–$2S$ transition. From test measurements with increased stray light we restrict such an effect to 0.4×10^{-15}. Also, atoms leaving the quench beam experience a low intensity region at the far wing of the Gaussian beam profile at which they are shifted but not quenched. We numerically simulate this effect by extending our MC simulation by a spatially dependent quench rate and an ac Stark shift due to the quench laser. We find no significant shift with an uncertainty of 0.8×10^{-15}.

The residual Zeeman shift of the $F = 1$, $m_F = \pm 1$ to $F' = 1$, $m_{F'} = \pm 1$ hyperfine transitions is ± 360 Hz/mT and, consequently, averages to zero for equal populations in both m_F components. In a dedicated experiment, we have measured the Zeeman shift to be below 0.38×10^{-15} by increasing and varying the applied magnetic field.

Following [21], we correct the shift due to blackbody radiation at 300(30) K which is $-4.1(1.2) \times 10^{-16}$. Measuring the temperature fluctuations of the power switching AOM with the fed rf power we find an upper limit for an associated frequency chirp at 1.1×10^{-16}. From a measurement of the power radiated from the rf discharge into the excitation region we can estimate a possible ac Stark effect below 1.2×10^{-17}.

Nonperfect mode matching to the cavity can give rise to a residual first order Doppler effect due to a weak running wave. With a measured finesse of 120 and a coupling efficiency of 75%, the power of this wave is estimated to be 10^{-4} of the power of the standing wave, giving rise to an additional Doppler broadened line with the same relative amplitude. With the laser beam divergence of 10^{-3} rad we derive upper limits on the position and width in order to estimate the maximum line pulling of 1.2×10^{-17}.

Estimating the shift due to line pulling by the $m_F = 0$ hyperfine component in a similar way we restrict it at 1.6×10^{-18}. A residual recoil shift can be limited by analysis of the observed Doppler broadening to be below 3.6×10^{-18}.

The uncertainty of the Cs fountain clock used for the absolute frequency measurement has been evaluated to 0.81×10^{-15} [22]. A conservative estimate of the height difference between clock and experiment contributes a gravitational redshift uncertainty of 7.7×10^{-17}. The uncertainty budget is summarized in Table I.

Summarizing all corrections and uncertainties we find the $1S$–$2S$ hyperfine centroid frequency to be

$$f_{1S\text{–}2S} = 2\,466\,061\,413\,187\,035\,(10)\ \text{Hz}.$$

This corresponds to a fractional frequency uncertainty of 4.2×10^{-15} and is in good agreement with our previous best measurement [3] but 3.3 times more accurate. A comparison of the previous two measurements along with

the current result is presented in Fig. 5. The excessive day to day scatter present in the 1999 and 2003 measurements has been attributed to a dye laser instability and has consequently been removed in the current measurement.

The authors thank E.A. Hessels for insightful discussions, M. Fischer for providing a second frequency comb, and T. Nebel and M. Herrmann for carefully reading the manuscript. J A. acknowledges support by the Marie Curie Intra European program, N K. from Presidential Grant No. MD-669.2011.8 and DFG Grant No. 436 RUS113/984/0-1, and T. W. H. from the Max Planck Foundation.

*Also at Menlo Systems GmbH, Martinsried, Germany.
†Also at P. N. Lebedev Physical Institute, Moscow, Russia. kolik@lebedev.ru
‡Also at Ludwig-Maximilians-University, Munich, Germany.

[1] F. Biraben, Eur. Phys. J. Special Topics **172**, 109 (2009).
[2] P. J. Mohr *et al.*, Rev. Mod. Phys. **80**, 633 (2008).
[3] M. Fischer *et al.*, Phys. Rev. Lett. **92**, 230802 (2004).
[4] B. Altschul, Phys. Rev. D **81**, 041701(R) (2010).
[5] G. Gabrielse, in *Fundamental Symmetries*, edited by P. Bloch, P. Pavlopoulos, and R. Klapisch (Plenum, New York, 1987), p. 59.
[6] ALPHA Collaboration, Nature Phys. **7**, 558 (2011).
[7] M. Niering *et al.*, Phys. Rev. Lett. **84**, 5496 (2000).
[8] N. Kolachevsky *et al.*, Opt. Lett. **36**, 4299 (2011).
[9] J. Alnis *et al.*, Phys. Rev. A **77**, 053809 (2008).
[10] S. Bize *et al.*, C.R. Physique **5**, 829 (2004).
[11] Th. Udem *et al.*, Opt. Lett. **23**, 1387 (1998).
[12] J. T. M. Walraven and I. S. Silvera, Rev. Sci. Instrum. **53**, 1167 (1982).
[13] C. G. Parthey *et al.*, Phys. Rev. Lett. **104**, 233001 (2010).
[14] L. Essen *et al.*, Nature (London) **229**, 110 (1971).
[15] N. Kolachevsky *et al.*, Phys. Rev. Lett. **102**, 213002 (2009).
[16] T. W. Hänsch *et al.*, Phys. Rev. Lett. **34**, 307 (1975).
[17] N. Kolachevsky *et al.*, Phys. Rev. A **74**, 052504 (2006).
[18] M. Haas *et al.*, Phys. Rev. A **73**, 052501 (2006).
[19] D. H. McIntyre *et al.*, Phys. Rev. A **39**, 4591 (1989).
[20] U. D. Jentschura *et al.*, Phys. Rev. A **83**, 042505 (2011).
[21] J. W. Farley and W. H. Wing, Phys. Rev. A **23**, 2397 (1981).
[22] ftp://ftp2.bipm.org/pub/tai/data/PFS_reports/syrte-fom_55344-55359.pdf.